Electronic Supplementary Material (ESI) for Physical Chemistry Chemical Physics.
This journal is © the Owner Societies 2018

Supplemental Information for the article "Towards a full quantitative description of single-molecule reaction kinetics in biological cells"

I. DETERMINATION OF THE EXPANSION COEFFICIENTS

To compute the coefficients a_n within the self-consistent approximation (SCA), we first substitute $\tilde{S}(r,\theta;p)$ defined in (4) into the modified boundary condition in (3), which gives

$$u_0'(\rho) + \sum_{n=0}^{\infty} a_n\, g_n'(\rho)\cos(n\theta) = \frac{Q}{R^2}\,\Theta(\varepsilon-\theta), \tag{S1}$$

where

$$g_n'(r) = \frac{\alpha_n}{L}\big[I_1(\alpha_n r/L)K_1(\alpha_n R/L) - K_1(\alpha_n r/L)I_1(\alpha_n R/L)\big]. \tag{S2}$$

Multiplying (S1) by $\cos(n\theta)$ (with $n = 0, 1, 2, \ldots$) and integrating over θ from 0 to π, one gets

$$Q = \frac{\pi R^2}{\varepsilon}\big(u_0'(\rho) + a_0 g_0'(\rho)\big), \tag{S3}$$

$$a_n = \frac{2Q}{\pi R^2 g_n'(\rho)}\,\frac{\sin n\varepsilon}{n} \quad (n = 1, 2, \ldots), \tag{S4}$$

so that

$$a_n = 2\,\frac{u_0'(\rho) + a_0 g_0'(\rho)}{g_n'(\rho)}\,\frac{\sin n\varepsilon}{n\varepsilon} \quad (n = 1, 2, \ldots). \tag{S5}$$

Consequently, $\tilde{S}(r,\theta;p)$ writes

$$\tilde{S}(r,\theta;p) = \frac{R^2}{D}\bigg(u_0(r) + a_0 g_0(r) + 2\big(u_0'(\rho) + a_0 g_0'(\rho)\big)\sum_{n=1}^{\infty}\frac{g_n(r)}{g_n'(\rho)}\,\frac{\sin n\varepsilon}{n\varepsilon}\,\cos(n\theta)\bigg). \tag{S6}$$

The coefficient a_0 (and hence, the trial current Q) remains a free parameter which is to be chosen in a self-consistent way. Within the SCA proposed in [1] (see also [2, 3] for more details on the adaption of this scheme to the first-passage phenomena) the closure relation is obtained by requiring that the mixed boundary condition in (2) holds not locally but *on average*.

For this purpose, we substitute this expression into (2) and integrate the resulting expression over θ from 0 to ε to get

$$a_0 = \frac{1-\eta}{s\, g_0(\rho)}\,, \tag{S7}$$

with η defined by (8). Combining these results, we get an approximate but explicit solution

$$\tilde{S}(r,\theta;p) = \frac{1}{p}\bigg(1 - \eta\,\frac{g_0(r)}{g_0(\rho)} + 2\eta\,\frac{g_0'(\rho)}{g_0(\rho)}\sum_{n=1}^{\infty}\frac{g_n(r)}{g_n'(\rho)}\,\frac{\sin n\varepsilon}{n\varepsilon}\cos(n\theta)\bigg), \tag{S8}$$

from which (7) follows.

II. NUMERICAL VALIDATION OF THE RESULTS OBTAINED WITHIN THE SCA

The proposed SCA provides an exact solution of the modified boundary value problem, in which the mixed Robin-Neumann boundary condition in (2) is substituted by the effective inhomogeneous Neumann condition in (3). To check the accuracy of this approximation and hence, of the resulting FPT distribution, we solve the original modified Helmholtz equation by a finite elements method (FEM) implemented in Matlab's PDEtool. Setting $\tilde{H}(r,\theta;p) = u(r/R,\theta;pR^2/D)$ we rewrite the modified Helmholtz equation in cylindrical coordinates as

$$(\partial/\partial r)r(\partial/\partial r)u + r\pi^2(R^2/L^2)(\partial^2/\partial\theta^2)u - rsu = 0, \tag{S9}$$

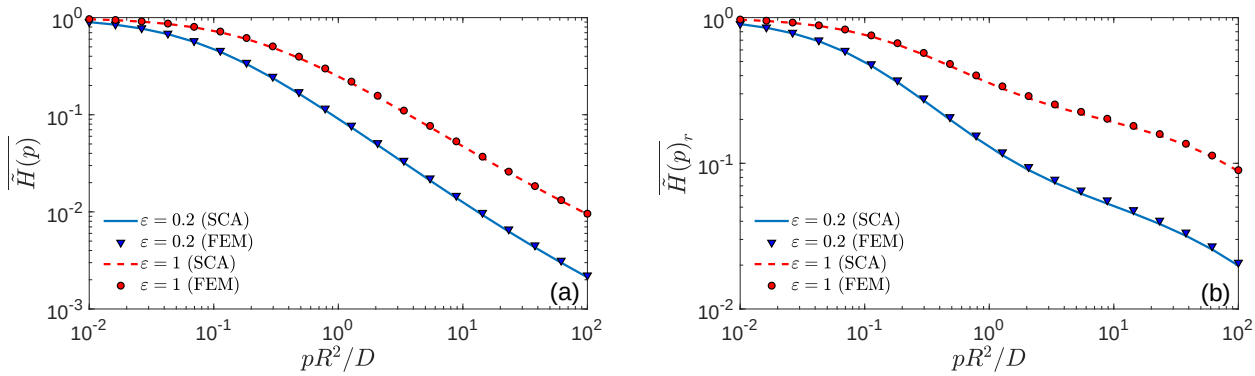

FIG. S1: Volume-averaged **(a)** and surface-averaged **(b)** Laplace-transformed FPT densities $\overline{\tilde{H}(p)}$ and $\overline{\tilde{H}(p)}_r$ as function of $s = pR^2/D$ for $L/R = \pi$, $\rho/R = 0.1$, $r/R = 0.2$, $\kappa = \infty$, and two values of ε indicated in the plot. Lines show (10) **(a)** and (11) **(b)** of our self-consistent approximation, in which the series in (9) is truncated to $N = 100$ terms. Symbols present a FEM numerical solution of the modified Helmholtz (S9), with mixed boundary condition (S10) with the maximal mesh size $h = 0.005$. Length and time scales are fixed by setting $R = 1$ and $R^2/D = 1$.

which has to be solved on the rectangular domain $(\rho/R, 1) \times (0, \pi)$ with Neumann boundary condition imposed everywhere except for the segment $(\rho) \times (0, \varepsilon)$, for which (2) reads

$$\left(u - \frac{D}{R\kappa}\frac{\partial u}{\partial r}\right)_{|r=\rho} = 1 \qquad (0 < \theta < \varepsilon). \tag{S10}$$

Once the solution u is found on mesh vertices, one can also compute its volume and surface averages. The volume-averaged quantity $\overline{\tilde{H}(p)}$ is obtained by a numerical integration of the solution over the computation domain, whereas the surface-averaged quantity $\overline{\tilde{H}(p)}_r$ is evaluated by first a linear interpolation of the solution to the vertical line at r and then by a numerical integration over this line.

The accuracy of the numerical solution of this problem and its averages is controlled by the maximal mesh size h, i.e., the largest allowed diameter of triangles of the mesh used to discretise the computational domain. In particular, the maximal mesh size should be much smaller than the length ε of the reactive segment. This condition limits the accessible target heights ε. In our numerical analysis, we set $h = 0.005$ that results in meshes with more than 200 000 triangles. It should be noted that since the numerical solution should be repeated for many values of p (or s), computations with even larger meshes (and thus smaller h and ε) become too time-consuming. Moreover, this long computation also prohibits using the Talbot algorithm for the Laplace inversion. Alternatively, the probability density $H(r, \theta; t)$ in time domain might be computed by solving directly the diffusion equation for the survival probability, but this solution would be even more time-consuming and limited to a relatively narrow range of times. For these reasons, we focus here on a numerical validation of the SCA only in the Laplace domain, i.e., checking the moment-generating function over a wide range of variation of the parameter p of the Laplace transform, instead of the probability density function itself. From a formal viewpoint, this is equivalent to validating the FPT distribution since both quantities are uniquely linked by the Laplace transform.

Figure S1 shows excellent agreement between the result based on the SCA and the FEM solution of the original mixed boundary value problem for $\varepsilon = 0.2$ and $\varepsilon = 1$ (we do not consider the case $\varepsilon = \pi$ for which the SCA yields the exact solution, see Section V of the SI). Moreover, the result of the SCA converges rapidly as the upper summation truncation N of the series in (9) increases. In particular, the results for $N = 50$ (not shown) and $N = 100$ are barely distinguishable. Small deviations at large p can be attributed to (i) inaccuracy of the FEM solution (and the consequent numerical integrations for getting volume and surface averages), and (ii) intrinsic small differences between the original and modified problems. Nevertheless, the quality of the SCA is quite impressive.

The SCA becomes particularly robust for imperfect reactions on the target. Figure S2 compares the SCA to the FEM solution for $\varepsilon = 0.2$ and several values of κ. The SCA predictions and FEM solutions are indistinguishable at the logarithmic scale. Lastly, as discussed in Ref. [2], the SCA is generally getting more accurate for smaller target size ε, smaller reactivity κ, and for starting points that are not too close to the target. Moreover, it was shown recently in Ref. [4], in which the self-propulsion velocity of catalytically-active colloids was studied by a similar method, that also for an arbitrary ε the SCA provides an accurate description and only slightly overestimates the numerical factors.

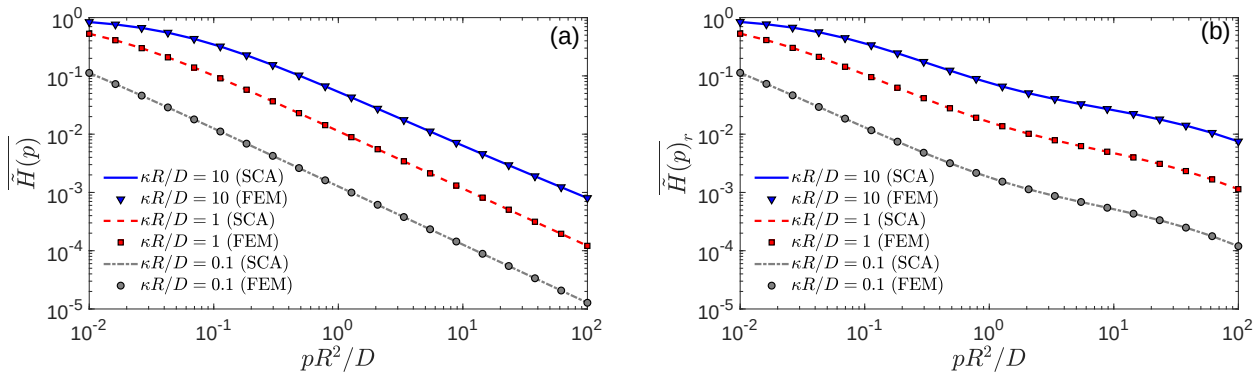

FIG. S2: Volume-averaged **(a)** and surface-averaged **(b)** Laplace-transformed FPT densities $\overline{\tilde{H}(p)}$ and $\overline{\tilde{H}(p)}_r$ as function of $s = pR^2/D$ for $L/R = \pi$, $\rho/R = 0.1$, $r/R = 0.2$, $\varepsilon = 0.2$, and three values of κ, indicated in the plot. Lines show (10) **(a)** and (11) **(b)** of our self-consistent approximation, in which the series in (9) is truncated to $N = 100$ terms. Symbols present a FEM numerical solution of the modified Helmholtz (S9), with mixed boundary condition (S10) with the maximal mesh size $h = 0.005$. Length and time scales are fixed by setting $R = 1$ and $R^2/D = 1$.

III. THE PROBABILITY DENSITY IN TIME DOMAIN

The Laplace-transformed probability density $\tilde{H}(r,\theta;p)$ and the related surface and volume-averaged quantities can be inverted by using the residue theorem. For this purpose, one searches for the poles of $\tilde{H}(r,\theta;p)$ in the complex plane $p \in \mathbb{C}$. In general, there are two groups of poles, which can be identified as (i) zeros of functions $g_n'(\rho)$ and (ii) zeros of the function $g_0(\rho)/\eta$.

(i) Introducing the auxiliary function

$$\hat{G}(z) \equiv -iz\Big(I_1(-iz\rho/R)K_1(-iz) - K_1(-iz\rho/R)I_1(-iz)\Big) = -\frac{\pi i}{2}z\Big(Y_1(z\rho/R)J_1(z) - J_1(z\rho/R)Y_1(z)\Big), \tag{S11}$$

one writes $g_n'(\rho) = \hat{G}(i\alpha_n R/L)/R$, where $\alpha_n = \sqrt{\pi^2 n^2 + pL^2/D}$. One can check that the function $\hat{G}(z)$ has infinitely many zeros all lying on the real axis. Since the Bessel functions obey

$$\begin{aligned} J_n(-x) &= (-1)^n J_n(x) \\ Y_n(-x) &= (-1)^n\big(Y_n(x) + 2iJ_n(x)\big) \end{aligned} \qquad (x > 0),$$

one deduces that $\hat{G}(-z) = -\hat{G}(z)$. We can thus focus only on the positive zeros of $\hat{G}(z)$ denoted as $\hat{z}_k$ (with $k = 1, 2, \ldots$). We relate them to the zeros of $g_n'(\rho)$:

$$p_{n,k} = -D\left(\frac{\hat{z}_k^2}{R^2} + \frac{\pi^2 n^2}{L^2}\right), \qquad \left(\begin{array}{l} n = 1, 2, \ldots \\ k = 1, 2, \ldots \end{array}\right). \tag{S12}$$

For each n, all the poles $p_{n,1}, p_{n,2}, \ldots$ are expected to be simple. In turn, it is possible to tune R and L to make some poles with different n coincide and thus be of the order higher than 1. At such poles, the computation of the residue would be more involved.

(ii) Similarly, we introduce the function

$$G_r(z) \equiv I_0(-izr/R)K_1(-iz) + K_0(-izr/R)I_1(-iz) = \frac{\pi i}{2}\Big(Y_0(zr/R)J_1(z) - J_0(zr/R)Y_1(z)\Big), \tag{S13}$$

to write $g_n(r) = G_r(i\alpha_n R/L)$. Note that this function is also antisymmetric: $G_r(-z) = -G_r(z)$. The poles of the function

$$\frac{\eta}{g_0(\rho)} = \frac{1}{g_0(\rho) - \big(\frac{\pi D}{\kappa\varepsilon} + \frac{L}{\pi}\mathcal{R}_\varepsilon\big)g_0'(\rho)}$$

are related to the zeros of the function

$$F(z) \equiv G_\rho(z) - \left(\frac{\pi D}{R\kappa\varepsilon} + \frac{L}{\pi R}\mathcal{R}_\varepsilon(z)\right)\hat{G}(z), \tag{S14}$$

where

$$\mathcal{R}_\varepsilon(z) = -\frac{2\pi R}{L}\sum_{n=1}^{\infty}\left(\frac{\sin n\varepsilon}{n\varepsilon}\right)^2 \frac{G_\rho\big(\sqrt{z^2-\pi^2n^2R^2/L^2}\big)}{\hat{G}\big(\sqrt{z^2-\pi^2n^2R^2/L^2}\big)}\,. \tag{S15}$$

Denoting the positive zeros of $F(z)$ as z_k, we get the poles as

$$p_{0,k} = -\frac{D}{R^2}z_k^2 \qquad (k=1,2,\ldots). \tag{S16}$$

Having identified all the poles, one can formally invert the Laplace transform by applying the residue theorem.

IV. LONG AND SHORT TIME ASYMPTOTICAL BEHAVIOUR OF THE FPT DENSITY

We here summarise the relations relevant for the calculation of the asymptotic behaviours of the FPT density.

Long-time behaviour

With $p \to 0$ we also have $s \to 0$, which then leads to $\alpha_n = \pi n + O(s)$ for $n > 0$ and $\alpha_0 = \sqrt{s}\,L/R$. We get

$$g_0(r) \simeq \frac{1}{\sqrt{s}}\left(1 + s\left(\frac{r^2}{4R^2} - \frac{1}{2}\ln(r/R)\right) + O(s^2)\right), \tag{S17}$$

so that

$$\frac{g_0(r)}{g_0(\rho)} \simeq 1 - \left(\frac{\rho^2-r^2}{4R^2} + \frac{\ln(r/\rho)}{2}\right)s + O(s^2), \tag{S18}$$

$$\frac{g_0'(\rho)}{g_0(\rho)} \simeq -s\frac{1-(\rho/R)^2}{2\rho} + O(s^2), \tag{S19}$$

$$\mathcal{R}_\varepsilon \simeq \mathcal{R}_\varepsilon(p=0) + O(s), \tag{S20}$$

$$\eta^{-1} \simeq 1 + p\overline{T}_\rho + O(p^2), \tag{S21}$$

where $\overline{T}_\rho$ from (14) is the surface-averaged MFPT studied in Ref. [3].

Short-time behaviour

The short-time behaviour corresponds to the limit $p \to \infty$, in which we get

$$\frac{g_n(\rho)}{g_n'(\rho)} \simeq -\frac{L}{\alpha_n}\frac{K_0(\alpha_n\rho/L)}{K_1(\alpha_n\rho/L)} \simeq -\frac{L}{\alpha_n}\left(1 - \frac{1}{2\alpha_n\rho/L} + \frac{3}{8(\alpha_n\rho/L)^2} + \ldots\right) \tag{S22}$$

and

$$\mathcal{R}_\varepsilon \simeq 2\pi\sum_{n=1}^{\infty}\left(\frac{\sin n\varepsilon}{n\varepsilon}\right)^2\left(\frac{1}{\alpha_n} - \frac{L}{2\rho\alpha_n^2} + \ldots\right). \tag{S23}$$

Setting $z = \sqrt{s}L/R$ we identify the leading part in the first term by writing

$$\mathcal{R}_\varepsilon \simeq 2\pi\sum_{n=1}^{\infty}\left(\frac{\sin n\varepsilon}{n\varepsilon}\right)^2\left(\frac{1}{z} - \frac{\pi^2n^2}{z\alpha_n(\alpha_n+z)} - \frac{L}{2\rho\alpha_n^2} + \ldots\right). \tag{S24}$$

The first term yields the leading contribution equal to $\frac{\pi(\pi-\varepsilon)}{\varepsilon}z^{-1}$, in virtue of the identity

$$\sum_{n=1}^{\infty}\left(\frac{\sin n\varepsilon}{n\varepsilon}\right)^2 = \frac{\pi-\varepsilon}{2\varepsilon}. \tag{S25}$$

The second sum in (S24) can be written as

$$\mathcal{R}_\varepsilon^{(2)} = -\frac{\pi^3}{z\varepsilon^2}\sum_{n=1}^{\infty}\frac{1-\cos 2n\varepsilon}{\pi^2 n^2 + z^2 + \alpha_n z} \simeq -\frac{\pi^3}{z\varepsilon^2}\sum_{n=1}^{\infty}\frac{1-\cos 2n\varepsilon}{\pi^2 n^2 + 2z^2}, \tag{S26}$$

where we substituted $\alpha_n \simeq z$ (for large z) in the denominator of the last term. Using the identity

$$\sum_{n=1}^{\infty}\frac{\cos(\pi n x)}{\pi^2 n^2 + z^2} = \frac{\cosh(1-x)z}{2z\sinh z} - \frac{1}{2z^2}, \tag{S27}$$

which is valid for $0 \le x \le 1$, we find

$$\mathcal{R}_\varepsilon^{(2)} \simeq -\frac{\pi^3}{z\varepsilon^2}\frac{\cosh(z\sqrt{2}) - \cosh(z\sqrt{2}(1-2\varepsilon/\pi))}{2\sqrt{2}z\sinh(z\sqrt{2})}. \tag{S28}$$

We emphasise that this relation is only valid for $\varepsilon \le \pi/2$. At large s (or z), one thus gets a very accurate approximation

$$\mathcal{R}_\varepsilon^{(2)} \simeq -\frac{\pi^3}{2\sqrt{2}z^2\varepsilon^2}\left(1 - e^{-2\sqrt{2}z\varepsilon/\pi}\right). \tag{S29}$$

Finally, in the third term of (S24) we approximate again $\alpha_n^2 \approx z^2$, which yields $-\frac{\pi(\pi-\varepsilon)L}{2\varepsilon\rho}z^{-2}$. Combining these results, we obtain

$$\mathcal{R}_\varepsilon \simeq \frac{\pi(\pi-\varepsilon)R}{\varepsilon L}s^{-1/2} - \mathcal{A}s^{-1} + O(s^{-\frac{3}{2}}), \tag{S30}$$

with

$$\mathcal{A} = \frac{\pi R^2}{\varepsilon L^2}\left(\frac{\pi^2}{2\sqrt{2}\varepsilon} + \frac{(\pi-\varepsilon)L}{2\rho}\right), \tag{S31}$$

in which we neglected the exponential correction in (S29).

From (S22), we also get

$$-\frac{g_0'(\rho)}{g_0(\rho)} \simeq \frac{\sqrt{s}}{R} + \frac{1}{2\rho} - \frac{R}{8\rho^2}s^{-1/2} + O(s^{-1}). \tag{S32}$$

Combining these results, we find the large s asymptotic behaviour of (8),

$$\eta \simeq \frac{\varepsilon}{\pi}\left[s^{1/2}\frac{D}{\kappa R} + \left(1 + \frac{D}{2\kappa\rho}\right) - \left(\frac{DR}{8\kappa\rho^2} + \frac{\pi R}{\sqrt{8}\varepsilon L}\right)s^{-1/2} + O(s^{-1})\right]^{-1}. \tag{S33}$$

When $\kappa = \infty$, (S33) becomes

$$\eta \simeq \frac{\varepsilon}{\pi} + \frac{\sqrt{D}}{2\sqrt{2}L}p^{-1/2} + O(p^{-1}). \tag{S34}$$

When the particles start from a cylindrical surface at r, to obtain (18) we need the large-s asymptotic relation

$$g_0(r) \simeq \frac{\cosh(\sqrt{s}(1-\frac{r}{R}))}{\sqrt{s}\sqrt{r/R}}\left(1 - \frac{\tanh(\sqrt{s}(1-\frac{r}{R}))}{8}(3 + R/r)s^{-1/2} + O(s^{-1})\right), \tag{S35}$$

from which we find the Laplace-transformed FTP density

$$\overline{\tilde{H}(p)}_r \simeq \eta\sqrt{\rho/r}\exp\left(-(r-\rho)\sqrt{p/D}\right)\left(1 + \sqrt{D}\frac{\sqrt{R/\rho} - \sqrt{R/r}}{8R}p^{-1/2} + O(p^{-1})\right) \tag{S36}$$

for $r < R$ and $p \to \infty$.

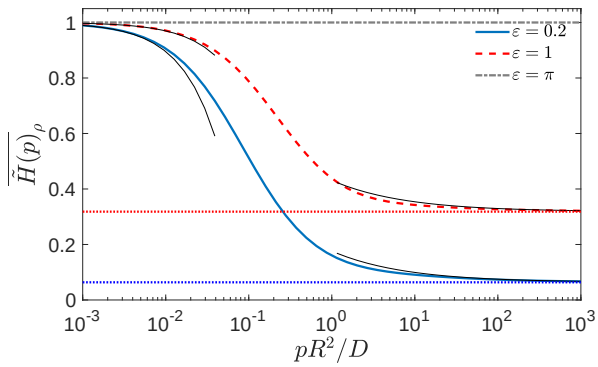

FIG. S3: Surface-averaged Laplace-transformed FPT density $\overline{\tilde{H}(p)}_\rho$ as function of $s = pR^2/D$ for $L/R = \pi$, $\rho/R = 0.1$, $\kappa = \infty$, and the three values of ε indicated in the plot. Thin solid lines show the asymptotic (S21) and (S34) as $s \to 0$ and $s \to \infty$, respectively. Dotted horizontal lines indicate the asymptotic limit ε/π of the FPT density as $s \to \infty$. Length and time scales are fixed by setting $R = 1$ and $R^2/D = 1$.

For $\kappa < \infty$, (S33) becomes

$$\eta \simeq \frac{\varepsilon}{\pi} \frac{\kappa}{\sqrt{D}} p^{-1/2} - \frac{\varepsilon}{\pi} \left(\frac{\kappa^2}{D} + \frac{\kappa}{2\rho} \right) p^{-1} + O(p^{-\frac{3}{2}}), \tag{S37}$$

which leads to (20).

Figure S3 illustrates the behaviour of the surface-averaged probability density $\overline{\tilde{H}(p)}_\rho$ for three target heights ϵ in the case of perfect reactions ($\kappa = \infty$). We observe that $\overline{\tilde{H}(p)}_\rho$ linearly approaches unity as $p \to 0$ (see (S21)) and reaches a constant ε/π, that is, the fraction of the target area, as $p \to \infty$. This is a consequence of the uniform surface average: particles that start from the target are immediately absorbed and thus not affected by diffusion-reaction processes. The case $\varepsilon = \pi$ corresponds to the fully absorbing inner cylinder, with $\overline{\tilde{H}(p)}_\rho = \eta = 1$.

V. TARGET ON THE WHOLE INNER CYLINDER

We consider the special case of the target extended to the whole inner cylinder (i.e., $\varepsilon = \pi$), for which $a_n = 0$ ($n > 0$), $\mathcal{R}_\pi = 0$, and thus the SCA yields

$$\tilde{S}(r, \theta; p) = \frac{1}{p} \left(1 - \eta \frac{g_0(r)}{g_0(\rho)} \right), \tag{S38}$$

with

$$\eta = \left(1 - \frac{g_0'(\rho)}{g_0(\rho)} \frac{D}{\kappa} \right)^{-1}. \tag{S39}$$

One can easily check that this is the *exact* solution of the original problem with a partially absorbing inner cylinder, i.e., this function satisfies the Robin boundary condition at $r = \rho$:

$$\left(D\partial_n \tilde{S} + \kappa \tilde{S} \right)_{r=\rho} = 0. \tag{S40}$$

In other words, our approximation becomes exact in the case $\varepsilon = \pi$.

From (S38), we also get the MFPT to the inner cylinder:

$$T = \frac{R^2 - \rho^2}{2\rho\kappa} + \frac{\rho^2 - r^2}{4D} + \frac{R^2 \ln(r/\rho)}{2D}, \tag{S41}$$

whereas its volume average reads

$$\overline{T} = \frac{R^2 - \rho^2}{2\rho\kappa} + \frac{R^2}{8D} \left(\frac{4 \ln(R/\rho)}{1 - (\rho/R)^2} - 3 + (\rho/R)^2 \right). \tag{S42}$$

The above exact solution suggests an interesting interpretation of the coefficient $\mathcal{R}_\varepsilon$ for the general case of an arbitrary ε. In fact, when the reactive region is only a part of the inner cylinder (i.e., $\varepsilon < \pi$), a diffusing particle will undergo multiple reflections by the remaining part of the inner cylinder until it reaches the target. If the target was composed of many small regions uniformly distributed over the inner cylinder, such a partially reactive boundary could be described by the Robin boundary condition over the whole inner cylinder, with an effective reactivity $\kappa_{\rm eff}$. In our case, the target is a single absorbing region, so that this homogenisation argument is *a priori* not applicable. Nevertheless, one can still introduce an effective, *apparent* reactivity by looking at the form of η in (8):

$$\frac{\pi}{\kappa\varepsilon} + \frac{L}{\pi D}\mathcal{R}_\varepsilon = \frac{1}{\kappa_{\rm eff}}\,. \tag{S43}$$

This relation can be thought of as an extension of the celebrated Collins-Kimball relations for the system under study (see [2, 3] for more details).

When the target is perfectly reactive, $\kappa = \infty$ and thus the effective reactivity represents the effect of the mixed Dirichlet-Neumann boundary condition: $\kappa_{\rm eff} = \frac{D\pi}{L\mathcal{R}_\varepsilon}$. If in addition the target is partially reactive, the overall reactivity is further reduced, as the particle has to reach the reactive part and then overcome the energy barrier. Interpreting the inverse of the reactivity as a "resistance", (S43) implies that the respective resistances enter additively, precisely as it happens in the classic analysis of Collins and Kimball.

VI. THE LIMIT $R \to \infty$

The distribution of the FPT remains well defined in the limit $R \to \infty$ when the outer cylinder moves to infinity. However, the MFPT diverges in this limit.

We get $\alpha_n = \sqrt{\pi^2 n^2 + pL^2/D}$, and $g_n(r) \simeq K_0(\alpha_n r/L) I_1(\alpha_n R/L)$, with an exponentially large factor $I_1(\alpha_n R/L)$. In particular, one finds

$$\tilde{S}_0(r;p) = \frac{1}{p}\left(1 - \frac{K_0(r\sqrt{p/D})}{K_0(\rho\sqrt{p/D})}\right) \tag{S44}$$

and

$$\frac{g_n(r)}{g_n'(\rho)} = -\frac{L}{\alpha_n}\,\frac{K_0(\alpha_n r/L)}{K_1(\alpha_n \rho/L)}\,. \tag{S45}$$

As a consequence, the Laplace-transformed pdf from (7) becomes

$$\tilde{H}(r,\theta;p) = \eta\,\frac{K_0(r\sqrt{p/D})}{K_0(\rho\sqrt{p/D})} + 2\eta\,L\sqrt{p/D}\,\frac{K_1(\rho\sqrt{p/D})}{K_0(\rho\sqrt{p/D})}\sum_{n=1}^{\infty}\frac{K_0(\alpha_n r/L)}{\alpha_n K_1(\alpha_n\rho/L)}\,\frac{\sin n\varepsilon}{n\varepsilon}\,\cos(n\theta), \tag{S46}$$

where

$$\eta^{-1} = 1 + \left(\frac{\pi D}{\kappa\,\varepsilon} + \frac{L}{\pi}\mathcal{R}_\varepsilon\right)\frac{\sqrt{p/D}\,K_1(\rho\sqrt{p/D})}{K_0(\rho\sqrt{p/D})} \tag{S47}$$

and

$$\mathcal{R}_\varepsilon = 2\pi\sum_{n=1}^{\infty}\frac{K_0(\alpha_n\rho/L)}{\alpha_n K_1(\alpha_n\rho/L)}\left(\frac{\sin n\varepsilon}{n\varepsilon}\right)^2. \tag{S48}$$

In particular, the surface average of (S46) yields

$$\overline{\tilde{H}(p)}_r = \eta\,\frac{K_0(r\sqrt{p/D})}{K_0(\rho\sqrt{p/D})}\,, \tag{S49}$$

whereas the volume average in (10) diverges as $R \to \infty$.

The particular case $\varepsilon = \pi$

The distribution of the FPT has already been studied in the particular case of a perfectly absorbing inner cylinder (i.e., $\varepsilon = \pi$ and $\kappa = \infty$). In this case, $\eta = 1$, and one retrieves the Laplace-transformed pdf of the FPT to a cylinder of radius ρ [5]. In particular, the distribution of the FPT in this particular case is known to be characterised by a power-law tail, $H_\pi(r;t) \propto 1/(t\ln^2(t))$ as $t \to \infty$, where subscript π signifies that this solution corresponds to $\varepsilon = \pi$, in which the vertical coordinate z (or θ) is irrelevant and thus the surface average does not change the solution. Levitz *et al.* [6] derived an approximation to $H_\pi(r;t)$ over the whole range of times (see below)

$$H_\pi(r;t) \simeq \begin{cases} \dfrac{r-\rho}{\sqrt{4\pi D t^3}} \exp\bigl(-\dfrac{(r-\rho)^2}{4Dt}\bigr) & (t < \rho^2/(2D)), \\ \dfrac{r/\rho - 1}{2t\bigl(1+\rho/\sqrt{2Dt}\bigr)\ln^2\bigl((r+\sqrt{2Dt})/\rho\bigr)} & (t > \rho^2/(2D)). \end{cases} \tag{S50}$$

This approximation is only valid for r close to ρ, i.e., when the particle starts in a vicinity of the inner cylinder.

We consider the more general case of a partially reactive inner cylinder (i.e., $\varepsilon = \pi$ and $\kappa < \infty$), for which (S46) becomes

$$\tilde{H}_\pi(r;p) = \frac{K_0(r\sqrt{p/D})}{K_0(\rho\sqrt{p/D}) + \frac{D}{\kappa}\sqrt{p/D}K_1(\rho\sqrt{p/D})}\,. \tag{S51}$$

Using the solution of an appropriate heat problem (see Ref. [7], p. 337), we can write the inverse Laplace transform as

$$H_\pi(r;t) = \frac{2\kappa}{\pi}\int\limits_0^\infty dq\, q\, e^{-Dtq^2}\,\frac{Y_0(qr)(qJ_1(q\rho)+hJ_0(q\rho)) - J_0(qr)(qY_1(q\rho)+hY_0(q\rho))}{(qJ_1(q\rho)+hJ_0(q\rho))^2 + (qY_1(q\rho)+hY_0(q\rho))^2}\,, \tag{S52}$$

where $h = \kappa/D$. In the long-time limit, the main contribution to the integral comes from $q \approx 0$. The asymptotic behaviour of the integrand function at $q \to 0$ yields

$$H_\pi(r;t) \simeq \frac{2\bigl(\frac{D}{\rho\kappa} + \ln(r/\rho)\bigr)}{t}\int\limits_0^\infty \frac{dz\, e^{-z}}{\pi^2 + \bigl(-\frac{2D}{\rho\kappa} + \ln(z\rho^2/(4Dt)) + 2\gamma\bigr)^2}\,, \tag{S53}$$

where $\gamma \approx 0.5772\ldots$ is the Euler constant. Discarding a slowly varying function $\ln(z)$ in the denominator, we find the following long-time asymptotic form

$$H_\pi(r;t) \simeq \frac{2\bigl(\frac{D}{\rho\kappa} + \ln(r/\rho)\bigr)}{t\bigl[\pi^2 + \bigl(\ln(\rho^2/(4Dt)) + 2\gamma - \frac{2D}{\rho\kappa}\bigr)^2\bigr]}\,, \tag{S54}$$

which exhibits a very slow decrease $1/(t\ln^2(t))$ as $t \to \infty$.

In the short-time limit, one uses the asymptotic behaviour of the integrand function as $q \to \infty$ to get

$$H_\pi(r;t) \simeq \frac{2\kappa\sqrt{\rho/r}}{\pi}\int\limits_0^\infty dq\, q\, e^{-Dtq^2}\,\frac{q\cos(q(r-\rho)) + h\sin(q(r-\rho))}{q^2+h^2}\,.$$

Ignoring the second term in the numerator, one gets the short-time asymptotic behaviour

$$H_\pi(r;t) \simeq \frac{\kappa\sqrt{\rho/r}}{\sqrt{\pi D t}}\exp\biggl(-\frac{(r-\rho)^2}{4Dt}\biggr) \quad (t \to 0). \tag{S55}$$

In the limit $\kappa \to \infty$ (perfect reactions), the exact solution in (S52) and its approximations (S54) and (S55) become respectively

$$H_\pi(r;t) = \frac{2D}{\pi}\int\limits_0^\infty dq\, q\, e^{-Dtq^2}\,\frac{Y_0(qr)J_0(q\rho) - J_0(qr)Y_0(q\rho)}{J_0^2(q\rho) + Y_0^2(q\rho)}\,, \tag{S56}$$

$$H_\pi(r;t) \simeq \frac{2\ln(r/\rho)}{t\bigl[\pi^2 + (\ln(\rho^2/(4Dt)) + 2\gamma)^2\bigr]} \quad (t \to \infty)\,, \tag{S57}$$

$$H_\pi(r;t) \simeq \frac{(r-\rho)\sqrt{\rho/r}}{\sqrt{4\pi D t^3}}\exp\biggl(-\frac{(r-\rho)^2}{4Dt}\biggr) \quad (t \to 0). \tag{S58}$$

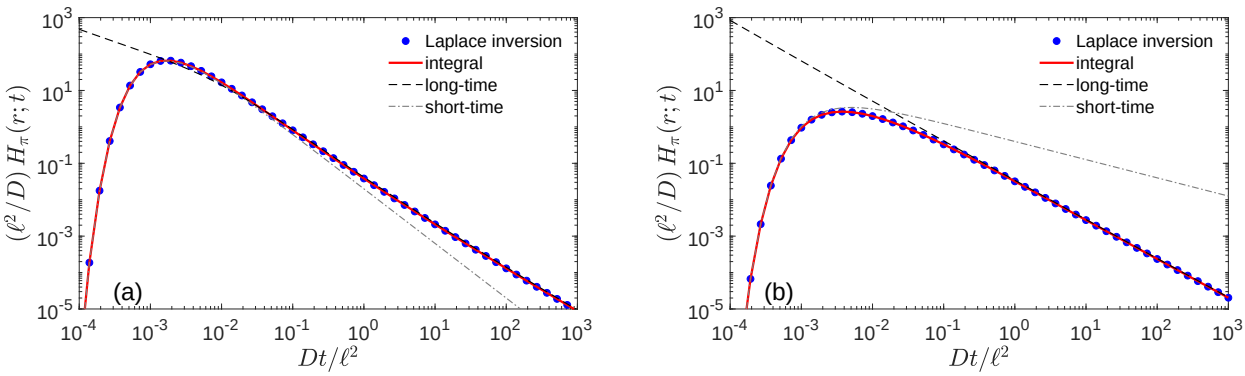

FIG. S4: The probability density $H_\pi(r;t)$ as function of t for $R=\infty$, $L/\ell=\varepsilon=\pi$, $\rho/\ell=0.1$, $\kappa=\infty$ **(a)** and $\kappa\ell/D=1$ **(b)**. The exact integral representation in (S52) (solid line) is compared to the numerical Laplace inversion of (S51) (circles) and to the long-time and short-time approximations (S54) and (S55). Length and time scales are fixed by setting $\ell=1$ and $\ell^2/D=1$, with an auxiliary length $\ell=L/\pi$.

As in Ref. [6], one can combine the short-time and long-time approximations to cover the whole range of times. If the maximum of $H_\pi(r;t)$ occurs in the validity range of (S58), one can easily get the most probable FPT by finding the zero of $\partial H_\pi(r;t)/\partial t$: $t_m=(r-\rho)^2/(6D)$. This value is three times smaller than that from (21) for a partially reactive target. The difference in the prefactor comes from different power law corrections to the common exponential function (cf. (S55) and (S58)): $t^{-3/2}$ for the perfectly reactive case and $t^{-1/2}$ for the partially reactive case.

Figure S4 illustrates the behaviour of the probability density $H_\pi(r;t)$. The exact integral representation in (S52) agrees perfectly with the numerical Laplace inversion of (S51) over a very broad range of times, confirming the high accuracy of the inversion procedure. When the inner cylinder is perfectly absorbing ($\kappa=\infty$), the long-time and short-time approximations ((S54) and (S55)) are very accurate and can be used to approximate the probability density over the whole range of times. For a partially reactive cylinder ($\kappa=1$), these approximations are less accurate but still good.

Comment on the approximation in (S50)

We briefly comment on the approximation in (S50) derived in Ref. [6]:

(i) we note that Eq. (1) in Ref. [6] is incorrect: the numerator and the denominator should be inter-changed. This typing error does not impact the consequent results.

(ii) the approximate Eq. (6) in Ref. [6] was derived under the simplifying assumption that the distance from the cylinder, $\delta=r-\rho$, is much smaller than the radius of the cylinder ρ. The same derivation without this assumption yields

$$H_\pi(r;t)=\frac{\ln(r/\rho)}{2t\bigl(1+r/\sqrt{2Dt}\bigr)\ln^2\bigl((r+\sqrt{2Dt})/\rho\bigr)}\,. \tag{S59}$$

When $\delta\ll\rho$, one has $\ln(r/\rho)=\ln(1+\delta/\rho)\simeq r/\rho-1$, and thus retrieves (S50), with r replaced by ρ in the denominator. As pointed out in Ref. [6], the approximation $H_\pi(r;t)$ has the correct normalisation by construction:

$$\int\limits_0^\infty dt\, H_\pi(r;t)=1. \tag{S60}$$

Since this approximation is only valid for long times, it can be completed by the short-time behaviour.

(iii) the approximation in (S50) and its extension in (S59) are slightly different from our asymptotic (S57) but they become identical in the long-time limit.

VII. THE LIMIT $L\to\infty$

In the limit $L\to\infty$, the capped annular domain transforms into an unbounded semi-infinite circular annulus: $\Omega=\{\mathbf{x}\in\mathbb{R}^3\ :\ \rho<\sqrt{x^2+y^2}<R,\ z>0\}$. In this case, the discrete summation variable $\xi=\pi n/L$ becomes

continuous, and one can replace sums by integrals. In particular, we get $\alpha_n/L = \sqrt{\xi^2 + p/D}$, and (9) becomes

$$\mathcal{R}_\varepsilon = \int\limits_0^\infty d\xi\, \Upsilon\big(\rho, \sqrt{\xi^2 + p/D}\big) \left(\frac{\sin \xi\epsilon}{\xi\epsilon}\right)^2, \tag{S61}$$

with

$$\Upsilon(r,\alpha) = -2 \frac{I_0(\alpha r) K_1(\alpha R) + K_0(\alpha r) I_1(\alpha R)}{\alpha\big(I_1(\alpha\rho) K_1(\alpha R) - K_1(\alpha\rho) I_1(\alpha R)\big)}\,. \tag{S62}$$

Since (8) yields

$$\eta \simeq -\frac{\pi}{L} \frac{g_0(\rho)}{g_0'(\rho)} \left(\frac{\pi D}{\kappa\epsilon} + \mathcal{R}_\varepsilon\right)^{-1}, \tag{S63}$$

the first term in (7) vanishes, whereas the second term transforms into

$$\tilde{H}(r,z;p) = \left(\frac{\pi D}{\kappa\epsilon} + \mathcal{R}_\varepsilon\right)^{-1} \int\limits_0^\infty d\xi\, \Upsilon\big(r, \sqrt{\xi^2 + p/D}\big) \frac{\sin \xi\epsilon}{\xi\epsilon} \cos \xi z. \tag{S64}$$

Due to the symmetry, this solution is also valid for an infinite circular annulus with the target region $(-\epsilon, \epsilon)$ on the inner cylinder. Note also that in the second limit $R \to \infty$, the function Υ reads

$$\Upsilon(r,\alpha) = \frac{2K_0(\alpha r)}{\alpha K_1(\alpha\rho)}\,. \tag{S65}$$

It is instructive to evaluate $\tilde{H}(r,z;p=0)$, which corresponds to the normalisation of the FPT. For a finite R, the integrals in (S61) and (S64) diverge as $p \to 0$, implying $\tilde{H}(r,z;p=0) = 1$, as expected. In contrast, when $R = \infty$, both integrals are finite, and thus $\tilde{H}(r,z;p=0) < 1$, i.e., the density $H(r,z;t)$ is not normalised to 1. This is the consequence of the transient character of the search process in three dimensions (when $L = R = \infty$). In this setting, $\tilde{H}(r,z;p=0)$ is the probability of finding the target.

In the limit $p \to \infty$, we have

$$\Upsilon(r,\alpha) \simeq \frac{2\sqrt{\rho/r}}{\alpha}\, e^{-\alpha(r-\rho)} \tag{S66}$$

so that

$$\mathcal{R}_\varepsilon \simeq \frac{\pi}{\epsilon\sqrt{p/D}}\,. \tag{S67}$$

For $0 < z < \epsilon$, we evaluate the leading contribution to the integral in (S64) and get

$$\tilde{H}(r,z;p) \simeq \sqrt{\rho/r}\, \frac{e^{-(r-\rho)\sqrt{p/D}}}{1 + \sqrt{pD}/\kappa}\,, \tag{S68}$$

which does not depend on ϵ and R in the leading order. Inverting this relation, we get the short-time asymptotic behaviour

$$H(r,z;t) \simeq \sqrt{\rho/r}\, e^{-(r-\rho)^2/(4Dt)} \left\{\frac{\kappa}{\sqrt{\pi D t}} - \frac{\kappa^2}{D} \mathrm{erfcx}\left(\left(\frac{r-\rho}{\sqrt{4Dt}} + \frac{\kappa\sqrt{t}}{\sqrt{D}}\right)^2\right)\right\}, \tag{S69}$$

where $\mathrm{erfcx}(x) = e^{x^2}\mathrm{erfc}(x)$ is the scaled complementary error function. In the perfectly reactive case $\kappa = \infty$, this expression is reduced to

$$H(r,z;t) \simeq \sqrt{\rho/r}\, \frac{r-\rho}{\sqrt{4\pi D t^3}}\, e^{-(r-\rho)^2/(4Dt)}\,. \tag{S70}$$

In the case $z \geq \epsilon$, the integral in (S64) requires a more subtle evaluation that we do not discuss here.

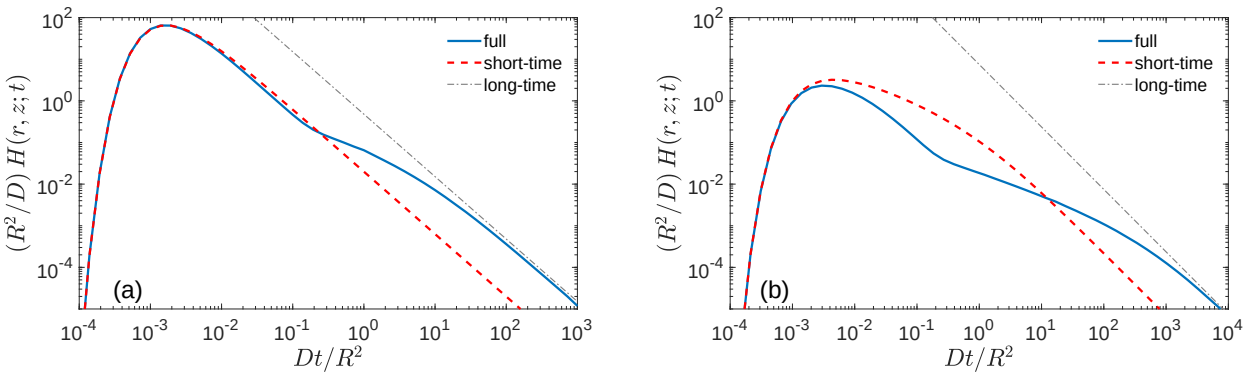

FIG. S5: The probability density $H(r,z;t)$ as function of t for $L=\infty$, $\epsilon/R=0.2$, $z/R=0.1$, $\rho/R=0.1$, $r/R=0.2$, $\kappa=\infty$ **(a)** and $\kappa R/D=1$ **(b)**. The numerical Laplace inversion of the integral representation in (S64) (solid line) is compared to its short-time behaviour (dashed line) in (S69) (for $\kappa R/D=1$) and (S70) (for $\kappa=\infty$) and long-time asymptotic relation in (S76) (dash-dotted line). Length and time scales are fixed by setting $R=1$ and $R^2/D=1$.

In the opposite limit $p\to 0$, the major contribution to integrals comes from $\xi\approx 0$. Since

$$\Upsilon(r,\alpha)\simeq\frac{4\rho}{\alpha^2(R^2-\rho^2)}+\frac{2\rho}{R^2-\rho^2}Y_r\qquad(\alpha\to 0),\tag{S71}$$

with

$$Y_r=\frac{r^2-R^2}{2}-\frac{R^2+\rho^2}{4}+R^2\ln(R/r)+\frac{R^2\rho^2\ln(R/\rho)}{R^2-\rho^2}\,,\tag{S72}$$

we deduce the leading contribution to $\mathcal{R}_\varepsilon$

$$\mathcal{R}_\varepsilon\simeq\frac{2\pi\rho}{(R^2-\rho^2)\sqrt{p/D}}+\frac{\pi\rho Y_\rho}{\epsilon(R^2-\rho^2)}\,.\tag{S73}$$

Similarly, we get for $0<z<\epsilon$

$$\int\limits_0^\infty d\xi\,\Upsilon\big(r,\sqrt{\xi^2+p/D}\big)\frac{\sin\xi\epsilon}{\xi\epsilon}\cos\xi z\simeq\frac{2\pi\rho}{(R^2-\rho^2)\sqrt{p/D}}+\frac{\pi\rho Y_r}{\epsilon(R^2-\rho^2)}\,,\tag{S74}$$

from which

$$\tilde{H}(r,z;p)\simeq 1-\sqrt{p/D}\,\frac{1}{2\epsilon}\left(\frac{D}{\kappa\rho}(R^2-\rho^2)+\frac{\rho^2-r^2}{2}+R^2\ln(r/\rho)\right),\tag{S75}$$

from which we deduce the long-time asymptotic behaviour

$$H(r,z;t)\simeq\frac{1}{\sqrt{4\pi Dt^3}}\,\frac{1}{2\epsilon}\left(\frac{D}{\kappa\rho}(R^2-\rho^2)+\frac{\rho^2-r^2}{2}+R^2\ln(r/\rho)\right).\tag{S76}$$

We retrieved the characteristic $t^{-3/2}$ decay of the FPT density for one-dimensional Brownian motion, which is supplemented by the geometric information on the target and the annular domain.

Figure S5 illustrates the probability density $H(r,z;t)$ as function of t for a semi-infinite circular annulus. One can see that both short-time and long-time asymptotic relations accurately capture this behaviour at small and large t, respectively.

[1] D. Shoup, G. Lipari and A. Szabo, Biophys. J. **36**, 697 (1981).

[2] D. S. Grebenkov and G. Oshanin, Diffusive escape through a narrow opening: new insights into a classic problem, Phys. Chem. Chem. Phys. **19**, 2723-2739 (2017).
[3] D. S. Grebenkov, R. Metzler, and G. Oshanin, Effects of the target aspect ratio and intrinsic reactivity onto diffusive search in bounded domains, New J. Phys. **19**, 103025 (2017).
[4] G. Oshanin, M. N. Popescu and S. Dietrich, Active colloids in the context of chemical kinetics, J. Phys. A: Math. Theor. **50** 134001 (2017).
[5] F. Spitzer, Some theorems concerning 2-dimensional Brownian motion, Trans. Am. Math. Soc. **87**, 187-197 (1958).
[6] P. Levitz, M. Zinsmeister, P. Davidson, D. Constantin, and O. Poncelet, Intermittent Brownian dynamics over a rigid strand: Heavily tailed relocation statistics, Phys. Rev. E **78**, 030102(R) (2008).
[7] H. S. Carslaw and J. C. Jaeger, Conduction of Heat in Solids, 2nd Ed. (Oxford University Press, 1959).